

INFORMATION TO USERS

This manuscript has been reproduced from the microfilm master. UMI films the text directly from the original or copy submitted. Thus, some thesis and dissertation copies are in typewriter face, while others may be from any type of computer printer.

The quality of this reproduction is dependent upon the quality of the copy submitted. Broken or indistinct print, colored or poor quality illustrations and photographs, print bleedthrough, substandard margins, and improper alignment can adversely affect reproduction.

In the unlikely event that the author did not send UMI a complete manuscript and there are missing pages, these will be noted. Also, if unauthorized copyright material had to be removed, a note will indicate the deletion.

Oversize materials (e.g., maps, drawings, charts) are reproduced by sectioning the original, beginning at the upper left-hand corner and continuing from left to right in equal sections with small overlaps. Each original is also photographed in one exposure and is included in reduced form at the back of the book.

Photographs included in the original manuscript have been reproduced xerographically in this copy. Higher quality 6" x 9" black and white photographic prints are available for any photographs or illustrations appearing in this copy for an additional charge. Contact UMI directly to order.

UMI

A Bell & Howell Information Company
300 North Zeeb Road, Ann Arbor MI 48106-1346 USA
313/761-4700 800/521-0600

PREVIEW

**DIRECT BONDING OF
METALS TO CERAMICS:
INTERFACE INVESTIGATIONS**

by

Victor Curicuta

A DISSERTATION

Presented to the Faculty of
The Graduate College at the University of Nebraska
Fulfillment of Requirements For the
Degree of Doctor of Philosophy

Major: Interdepartmental Area of Engineering
(Chemical & Materials Engineering)

Under the Supervision of Professor Dennis R. Alexander

Lincoln, Nebraska

August, 1998

UMI Number: 9903763

PREVIEW

UMI Microform 9903763
Copyright 1998, by UMI Company. All rights reserved.

**This microform edition is protected against unauthorized
copying under Title 17, United States Code.**

UMI
300 North Zeeb Road
Ann Arbor, MI 48103

©1998

ALL RIGHTS RESERVED

**DIRECT BONDING OF
METALS TO CERAMICS:
INTERFACE INVESTIGATIONS**

Victor Curicuta, Ph.D.

University of Nebraska, 1998

Advisor: Dennis R. Alexander

There is a growing interest in metal/ceramic bonding for a wide range of applications from electronic packaging to biomedical implants. In this research work, results are reported for direct bonding of copper to ceramic (e.g., Al_2O_3 and ZrO) in a furnace under inert atmosphere (e.g., N_2 and Ar_2). Other, metals such as Cu, Ni, SS-316 were directly bonded to ceramics (e.g., $\alpha\text{-Al}_2\text{O}_3$, sapphire) using laser heating (e.g., 247 nm and $10.6\text{ }\mu\text{m}$ wavelengths) in the presence of N_2 atmosphere. Cu flakes have been bonded to industrial alumina ceramic and sapphire in the presence of methyl, ethyl and isopropyl alcohols using a CO_2 laser. All these experiments were performed by heating the metal or metal-organic media member for a sufficient time in order to create a metal-metal oxide eutectic melt at the interface with the ceramic substrate.

Thermal wave imaging (TWI) was used to investigate the bonding at the metal/ceramic interface. It was found that the method of direct bonding of metals to ceramics using lasers performed better than the furnace. The properties of the copper bonded layer on alumina ceramic was investigated using scanning electron microscopy (SEM). Also, the elemental distribution at the metal/ceramic interface was analyzed, using energy dispersive x-ray spectroscopy (EDS). With the help of x-ray diffraction (XRD), the phase present at the copper/industrial alumina ceramic interface was determined to be CuAl_2O_4 . This was different from the CuAlO_2 phase found at the copper/sapphire interface for the furnace

bonding case. Transmission electron microscopy (TEM) and high resolution transmission electron microscopy (HRTEM) was also used to investigate the aspects of metal/ceramic interfaces. It was found that the samples processed by furnace heating and by laser beam heating have a diffused transition interface. The electron diffraction patterns revealed the phase present at the interface ($\text{Cu}/\alpha\text{-Al}_2\text{O}_3$) to be a cubic one, with the CuAl_2O_4 crystallographic structure. The TEM images show that the samples heated using excimer laser have an amorphous top copper layer. The HRTEM images of the samples heated with the excimer laser beam under N_2 atmosphere revealed that the inter-atomic spacing at the $\text{Cu}/\alpha\text{-Al}_2\text{O}_3$ interface region to be 0.365 nm in average. In order to investigate inter-diffusion between the copper layer and the sapphire and also to measure the percentage of diffused of copper in sapphire, Rutherford backscattering spectroscopy (RBS) was performed. Based on heat transfer theory and on diffusion theory, a model was derived to explain and predict the behavior of furnace and laser beam bonding of metals to ceramics. The predictions of the model were in agreement with the experimental percentage values of diffused copper in sapphire obtained in the RBS investigations. Experimental investigations and the theoretical model concluded that the direct bonding phenomenon is a thermal effect. The direct bonding phenomenon is similar to transient liquid phase bonding (TLP). The major advantage of direct bonding is that no filler element is required between the metallic member and the ceramic substrate. Finally, the method of direct bonding of metals to ceramics using laser beam is capable of directly drawing a metallic pattern on a ceramic substrate.

Acknowledgments

I like to dedicate this work to Ilinca (Coca) and Nolan.

I am deeply indebted to many individuals for their help in the completion of this work. Without their help this dissertation could not have been completed.

I would first like to thank my advisor, Dr. Dennis R. Alexander, for his support and advice. Also, I would like to thank, Dr. Robert J. DeAngelis and Dr. Brian W. Robertson for their help, advice and discussions. For the RBS investigation which was performed at the California Institute of Technology, I appreciate the help of Dr. E.A. Kolawa and S. Gasser. I would like to thank to Dr. Dana E. Poulain for computer debugging help and information. I am indebted for the help and discussions regarding Matlab software to Joseph K. Krause. I appreciate the help of Dr. Yi Liu with the TEM and HRTEM. I want to thank to David Doerr and Mark Rohlf for their helpful discussions and with computer work. I appreciate the help of Nek Debry with the sputtering work. Credit should be given to Brian E. Jones for x-ray diffraction assistance.

Preface

The purpose of this dissertation is first to improve furnace bonding of metals to ceramics and to introduce a new method using a laser for heating. The second objective is to investigate and characterize the direct bonding interface phenomenon by comparing the furnace direct bonding with that obtained by direct laser bonding. In order to characterize the interface, the studies include: thermal wave imaging (TWI), x-ray diffraction (XRD), scanning electron microscopy (SEM), electron dispersive x-ray spectroscopy (EDS), high-resolution transmission electron microscopy (HRTEM) and Rutherford backscattering spectroscopy (RBS) methods. A computer model based on heat transfer and diffusion phenomena was developed to help interpret the metal/ceramic interface diffusion and bonding phenomenon. Supporting information has been included as appendices.

Table of Contents

Acknowledgments	i
Preface	ii
Table of Contents	iii
List of Figures	vi
List of Tables	xiv
1 Introduction	1
1.1 Problem Foundation	1
1.1.1 <i>Direct Bonding of Metals to Ceramics</i>	2
1.2 Furnace Bonding Method	4
1.3 Bonding of Metals to Ceramics using Lasers	9
1.3.1 <i>Bonding of Metals to Ceramics using CO₂ laser heating.</i>	11
1.3.2 <i>Bonding of Metals to Ceramics using an EXCIMER laser</i>	19
1.4 Conclusions from the Experimental Direct Bonding of Metals to Ceramic	22
1.5 References	22
2 Investigation of Metal/Ceramic Direct Bonding	26
2.1 Thermal Wave Imaging of Metal/Ceramic Direct Bonding	26
2.2 X-Ray Diffraction Investigation	29
2.3 Phase Identification of Bonding by XRD	30
2.3.1 <i>Phase Identification for Copper-Alumina Samples</i>	30

2.3.2	<i>Interface Phase Identification for Copper-Alumina Samples</i>	34
2.4	Conclusions From the XRD Investigation	40
2.5	Scanning Electron Microscopy (SEM) and X-Ray Microanalysis Investigation	44
2.5.1	<i>SEM and Energy-Dispersive Spectrometry (EDS) Samples Investigation</i>	46
2.5.2	<i>Discussion of the SEM Direct Bonding Investigation</i>	49
2.6	Transmission Electron Microscopy (TEM) Investigation	54
2.6.1	<i>Phase Identification</i>	56
2.6.2	<i>Crystal Symmetry and Orientation Determination</i>	59
2.7	Imaging Modes of TEM Analysis	60
2.7.1	<i>High-Resolution Image Simulation and Analysis</i>	61
2.7.2	<i>Specimens Preparation</i>	67
2.7.3	<i>Discussion of the TEM Investigation of Direct Bonding Metal to Ceramic</i>	70
2.7.4	<i>Conclusion of the TEM Investigation of Direct Bonding Metal to Ceramic</i>	74
2.8	Rutherford Backscattering (RBS) Investigation	78
2.8.1	<i>RBS Theory</i>	78
2.8.2	<i>Reasons for using RBS Investigation.</i>	82
2.8.3	<i>RBS Sample Preparation</i>	83
2.8.4	<i>RBS Samples Investigation</i>	84
2.8.5	<i>Conclusions of RBS Samples Investigation</i>	98
2.9	References	99
3	Theoretical Considerations of Direct Bonding of Metals to Ceramics . .	101
3.1	Introduction	101
3.2	General Model for Furnace Direct Bonding of Metals to Ceramics .	101
3.2.1	<i>Modeling of Furnace Direct Bonding of Copper to Ceramic</i>	103
3.3	General Model for Laser Direct Bonding of Metals to Ceramics . .	108

3.3.1	<i>Modeling of Excimer Laser Beam Direct Bonding of Metal to Ceramic</i>	126
3.3.2	<i>Modeling of CO₂ Laser Beam Direct Bonding of Metal to Ceramic</i>	133
3.4	Interpretation of Theoretical Modeling	140
3.5	References	143
4	Conclusions	146
5	Recommendations for Future Work	148
5.1	References	149
A	TEM	150
A.1	Cu Crystallographic Data File	150
A.2	Al₂O₃ Crystallographic Data File	151
B	RBS	152
B.1	Kinematic Factor	152
B.2	Scattering Cross Section Equation	152
B.3	RBS List of Surface Energy Positions for the Relevant Elements	153
B.4	Thermodynamic and Optical Properties of Sapphire and Copper	153
B.5	References	153
C	Data Analysis Software	156
C.1	Direct Bonding of Copper to Sapphire Program for Furnace	156
C.2	Direct Bonding of Copper to Sapphire Program for Excimer Laser	159
C.3	Direct Bonding of Copper to Sapphire Program for CO₂ Laser	165
C.3.1	<i>Subroutine Program to Generate the Fonts for the Plots</i>	170

List of Figures

1.1	Phase diagram of the Cu - O system.	3
1.2	Experimental set-up for direct bonding in a furnace.	5
1.3	Examples of direct bonding of ZrO (6.5 mm thick) - Cu (0.254 mm thick) - Al ₂ O ₃ (1.4 mm thick) - Cu (0.254 mm thick) a), Al ₂ O ₃ (2.5 and 1.4 mm thick) - Cu (0.635 mm thick) b) and Al ₂ O ₃ (1.4 mm thick) - Cu (0.254 mm thick) c) using a furnace and 99.998% pure nitrogen gas.	7
1.4	Experimental set-up for direct bonding using a CO ₂ laser beam.	12
1.5	Experimental set-up for direct bonding using a focused CO ₂ laser beam. . .	17
1.6	Experimental set-up for direct bonding using a focused excimer laser beam or a CO ₂ laser beam.	20
1.7	Images of the experimental set-up for direct bonding using a focused excimer laser beam a) and stainless steel chamber b).	21
1.8	Samples of copper bonded to ceramic with a laser in an inert atmosphere. .	23
2.1	Schematic diagram of thermal wave detection of macrodefects at bonded interfaces.	27

2.2	Metal-bonded ceramic samples - pictures and thermal wave images. Copper directly bonded on ceramic samples a) and the corresponding thermal wave image at the interface metal/ceramic b). The sample 1) is a direct bonded sandwich of ZrO-Cu foil-Al ₂ O ₃ -Cu foil in furnace under the nitrogen atmosphere, sample 2) is a direct bonded sandwich of Al ₂ O ₃ -Cu foil in furnace under the nitrogen atmosphere and the samples 3), 4), 5) are direct bonded samples of Cu foil on Al ₂ O ₃ using a CO ₂ laser beam under the nitrogen atmosphere. The yellow and pink spots are the defects at the interface metal/ceramic.	28
2.3	XRD spectra of Cu 2,000 Å thick sputter deposited on sapphire (SPU) processed under N ₂ atmosphere in furnace (FUR), using a KrF excimer laser beam (248nm N), and a CO ₂ laser beam, with the initial Cu layer covered with carbon (10.6 N 2) and with the initial Cu layer not covered with carbon (10.6 N).	31
2.4	XRD spectra of Cu 2,000 Å thick sputter deposited on sapphire (SPU) processed in air using a KrF excimer laser beam (248nm A), and a CO ₂ laser beam, with the initial Cu layer covered with carbon (10.6 A 2) and with the initial Cu layer not covered with carbon (10.6 A).	33
2.5	XRD spectrum (0.5 step size) of the interface uncovered by etching the copper layer for the bonded copper/alumina ceramic in the furnace under a nitrogen atmosphere.	35
2.6	The software double identification of the same XRD peak (0.006° step size) for bonded copper/alumina ceramic in the furnace under a nitrogen atmosphere. The interface was uncovered by etching the copper layer.	36
2.7	The software double identification of the same XRD peak (0.006 step size) for bonded copper/alumina ceramic in furnace under nitrogen atmosphere. The interface was uncovered by etching the copper layer.	37

2.8	The software identification of XRD peak (0.006° step size) for bonded copper/alumina ceramic in furnace under nitrogen atmosphere. The interface was uncovered by etching the copper layer.	38
2.9	Software identification of the XRD peak (0.006° step size) for bonded copper/alumina ceramic in the furnace under a nitrogen atmosphere. The interface was uncovered by peeling off the copper layer.	39
2.10	XRD spectrum (40 KV, 20 mA, 0.02° steps/2sec.) of 1-5 μm copper powder 99% purity bonded on alumina ceramic using 248 nm excimer laser under the nitrogen atmosphere. Non labeled peaks are alumina and Cu peaks. As we see only the CuAl_2O_4 phase was identified as being present.	41
2.11	XRD spectrum (40 KV, 30 mA, 0.02° steps/2sec.) of 1-5 μm copper powder 99% purity bonded on industrial alumina ceramic using 248 nm excimer laser beam (In c 248nm) and using 10.6 μm CO_2 laser beam (In c 10.6 EDA 8h) under nitrogen atmosphere. The sample (In c 10.6 EDA 8h) was etched for 8 hours in EDA solution of pH 10 after laser processing. Non labeled peaks are Cu and Al_2O_3 peaks. As we see only the CuAl_2O_4 phase was identified as being present.	42
2.12	XRD spectrum (40 KV, 30 mA, 0.02 steps/2sec.) of Cu 2,000 Å thick sputter deposited on sapphire and processed in furnace (FUR c sp), using 248 nm excimer laser beam under N_2 atmosphere (248nm N c sp) and using 248 nm excimer laser beam in air (248nm A c sp). All the samples were etched in sodium phosphate solution. As we see only the CuAlO_2 phase was identified as being present.	43

2.13	The SEM image below corresponds to the sample geometry sketched above. The image came from transversal cross section of Cu flakes (1-5 μm and 99% purity) direct bonded using excimer laser ($\lambda = 248\text{ nm}$) under nitrogen atmosphere. Transversal cross section area was final polished by lapping on 0.5 μm diamond disk.	47
2.14	a) EDS for transverse cross section of Cu flakes (1-5 μm and 99% purity) direct bonded using excimer laser ($\lambda = 248\text{ nm}$) under nitrogen atmosphere. The final polishing step to flatness of this cross-section used lapping on 0.5 μm diamond disk.	48
2.15	From top to bottom low a) and high b) magnification SEM image of transverse cross section of Cu flakes (1-5 μm and 99% purity) directly bonded to alumina ceramic (97% purity) using CO_2 laser ($\lambda = 10.6\text{ }\mu\text{m}$) under nitrogen atmosphere. The final polish of the cross section was done by lapping on a 0.5 μm diamond abrasive disk.	50
2.16	Low magnification (top) and high magnification (bottom) SEM images of transverse cross section of SS-316 powder (1-5 μm grain size) directly bonded to alumina ceramic (97% purity) using CO_2 laser beam under nitrogen atmosphere. The final polish of the cross section was done by lapping on a 0.5 μm diamond abrasive disk.	51
2.17	EDS for transverse cross section of SS-316 powder (1-5 μm grain size) directly bonded to alumina ceramic (97% purity) using CO_2 laser beam under nitrogen atmosphere.	52
2.18	SS-316 powder (1-5 μm grain size) directly bonded to alumina ceramic (97% purity) using CO_2 laser beam under nitrogen atmosphere. BSEM image a) and EDS on diverse locations on the surface of SS-316 powder direct bonded on alumina ceramic b), c).	53

2.19 TEM samples preparation phases from the cutting phase a) to the final dimpled and ion milled phase b).	68
2.20 Cu/Al ₂ O ₃ interface TEM images of Cu bonded on industrial alumina ceramic under N ₂ atmosphere and processed in furnace a) and with the laser beam of $\lambda = 10.6 \mu\text{m}$ b) and $\lambda = 248 \text{ nm}$. c)	71
2.21 BF TEM negative image of directly bonded of Cu foil on alumina ceramic under N ₂ atmosphere in furnace a). The CBED pattern on Cu region b). The corresponding CBED at the interface d) shows a large cubic like structure that can come from CuAl ₂ O ₄ phase. The CBED pattern on α -Al ₂ O ₃ region c).	73
2.22 DF TEM a) and BF TEM b) negative images for direct bonding of Cu flakes on alumina ceramic under N ₂ atmosphere using an excimer laser (248 nm wavelength). The corresponding SAED at the interface c) shows a cubic like phase that might correspond to come from CuAl ₂ O ₄ . On the Cu side d) SAED shows ring patterns that reveal a nanosize region caused by the laser beam interaction with the material.	75
2.23 Enlarged DF TEM image of the interface region for direct bonding of Cu flakes on alumina ceramic under N ₂ atmosphere using an excimer laser (248 nm wavelength). The nanosize particles formation can be distinguished on the copper region.	76
2.24 HRTEM images of direct bonding of Cu flakes on alumina ceramic under N ₂ atmosphere using an excimer laser (248 nm wavelength). HREM image of presumed CuAl ₂ O ₄ phase a) and of the inter-diffusion interface region CuAl ₂ O ₄ / α -Al ₂ O ₃ b).	77
2.25 Schematic diagram of a typical RBS system.	79
2.26 Schematic diagram of a typical RBS wider peak effect produced by sample tilt.	86

2.27 Schematic diagram of a typical RBS spectrum shift as a function of element position in sample.	87
2.28 RBS plot of the copper sputtered on sapphire at 7° and 60° tilt to sample surface normal.	88
2.29 RBS plots of the sapphire/Cu sample heated in furnace and investigated at 7° and 60° tilt to the surface normal.	90
2.30 RBS plots of the sapphire/Cu sample heated with a single pulse excimer laser beam at 248 nm (KFr) wavelength in N ₂ (248N) and ambient (248A) atmosphere and was investigated at 7° tilt to the surface normal.	91
2.31 RBS plots of the sapphire/Cu sample heated with a single pulse excimer laser beam at 248 nm (KFr) wavelength in N ₂ (248N) and ambient (248A) atmosphere and was investigated at 60° tilt to the surface normal.	92
2.32 RBS plots of the sapphire/copper/carbon sample heated with a CO ₂ laser beam in N ₂ (10.6N) and ambient (10.6A) atmosphere and investigated at 7° tilt angle of sample to the surface normal.	94
2.33 RBS plots of the sapphire/copper/carbon sample heated with a CO ₂ laser beam in the N ₂ atmosphere and investigated at 7° and 45° tilt angles of sample to the surface normal.	95
2.34 Schematic diagram of the RBS effect of smoothing at the low energy edge a) and of a typical RBS effect of surface roughening b).	96
2.35 RBS plots of the sapphire/copper/carbon sample heated with a CO ₂ laser beam in the N ₂ (10.6 N2) and ambient (10.6 A2) atmosphere and investigated at 7° tilt to the surface normal.	97
3.1 The curve fit (square marks) of furnace temperature (circle marks) from room temperature to the bonding temperature.	102

3.2	Temperature in the Cu-sapphire sample processed in a furnace under an inert atmosphere as a function of process time.	104
3.3	Cu diffusion coefficients in sapphire for a sample processed in a furnace under an inert atmosphere as a function of process time.	105
3.4	Diffusion length of Cu in sapphire for the sample processed in furnace under inert atmosphere as a function of process time.	106
3.5	Percentage of diffused copper for the sample processed in furnace under inert atmosphere as a function of time and depth in sapphire.	107
3.6	Theoretical heat transfer model for CO ₂ laser heating case a) and for excimer laser heating case b) of a finite region (copper) and a semi infinite region (alumina) in perfect thermal contact.	113
3.7	Thermal conductivity of Cu and polycrystalline Al ₂ O ₃ as a function of temperature.	124
3.8	Specific heat of Cu and polycrystalline Al ₂ O ₃ as a function of temperature.	125
3.9	Temperature of sample copper layer surface as a function of time for the single pulse laser beam interaction ($\lambda = 248$ nm and 17.5 ns average FWHM).	127
3.10	Surface temperature variation caused by a single pulse interaction of laser energy ($\lambda = 248$ nm and 17.5 ns average FWHM) with the sample copper surface.	128
3.11	Temperature in copper as a function of copper depth and time caused by the single pulse interaction of the laser beam ($\lambda = 248$ nm and 17.5 ns average FWHM) with the sample copper surface.	129
3.12	Temperature in sapphire as a function sapphire depth and time caused by the single pulse interaction of laser beam ($\lambda = 248$ nm and 17.5 ns average FWHM) with the sample copper surface.	130

3.13	Diffusion length of copper in sapphire as a function of depth in sapphire and function of time caused by the single pulse interaction of laser beam ($\lambda = 248$ nm and 17.5 ns average FWHM) with the sample copper surface. . . .	131
3.14	Percentage of diffused copper in sapphire as a function of depth in sapphire and time caused by the single pulse interaction of laser beam ($\lambda = 248$ nm and 17.5 ns average FWHM) with the sample copper surface.	132
3.15	Temperature of sample copper layer surface as a function of time for the CO ₂ laser beam interaction (CW, $\lambda = 10.6$ μ m).	134
3.16	Surface copper layer temperature variation caused by the CO ₂ laser beam interaction (CW, $\lambda = 10.6$ μ m) with the sample copper surface.	135
3.17	Temperature in copper as a function of copper depth and time caused by the CW CO ₂ laser beam interaction ($\lambda = 10.6$ μ m) with the sample copper surface.	136
3.18	Temperature in sapphire as a function sapphire depth and time caused by the CW CO ₂ laser beam interaction ($\lambda = 10.6$ μ m) with the sample copper surface.	137
3.19	Diffusion length of copper in sapphire as a function of depth in sapphire and function of time caused by the CW CO ₂ laser beam interaction ($\lambda = 10.6$ μ m) with the sample copper surface.	138
3.20	Percentage of diffused copper in sapphire as a function of depth in sapphire and time caused by the CW CO ₂ laser beam interaction ($\lambda = 10.6$ μ m) with the sample copper surface.	139
3.21	Hypothetical binary phase diagram with eutectic point a) and different stages during heating cycle of direct bonding metals to ceramics b) where T_B is bonding temperature and T_M is melting point of metallic material.	141

List of Tables

1.I	Conditions for furnace direct bonding of copper to ceramics.	8
1.II	Al ₂ O ₃ /Cu samples and bonding results for CO ₂ laser beam of 11 mm diameter.	13
1.III	Experimental conditions for the laser direct bonding of 2,000 Å sputtered Cu on sapphire.	15
1.IV	Experimental conditions for the optimized laser direct bonding of metals to ceramics.	18
B.I	List of surface energy positions for different elements, at beam energy 2 MeV.154	
B.II	Thermodynamic and optical property of sapphire and copper.	155

Chapter 1

Introduction

Understanding the relationship among processing, phase structure, and properties of the metal/ceramic interfaces is becoming increasingly important as performance requirements demand the use of metal/ceramic composites in applications such as electronic devices, high temperature aircraft structures, and biomedical implants. In metal/ceramic composites, the overall composite properties depend critically on the properties of the metal/ceramic interface. Also, in recent years lasers are used in manufacturing plants for ablation, cutting and welding, and become more competitive with traditional manufacturing method systems. There also appears to be an advantage in using a laser in the metal/ceramic bonding process.

1.1 Problem Foundation

The original justification for this work came from a need to improve and to understand the metal/ceramic bonding process. In this work the improvement of directly bonding of metals to ceramics was studied by using a simple inert atmosphere during the bonding process. This study also includes a rapid and accurate bonding method using laser beam heating with an inert atmosphere. Finally, to understand the metal/ceramic interface reaction phenomenon samples from both the furnace and laser processes were investigated using non-destructive techniques such as thermal wave echo imaging (TWI), scanning electron microscopy and transmission electron microscopy (SEM, TEM), x-ray diffraction (XRD) and Rutherford backscattering spectroscopy (RBS) methods.

1.1.1 *Direct Bonding of Metals to Ceramics*

The method of direct bonding of metals to ceramics was first implemented in the 1970's by Babcock et al.¹ and has undergone minor changes as the technology has grown. The basic process comprises placing a metal member such as copper in contact with a non-metallic substrate such as alumina and then heating in a furnace to a temperature slightly below the melting point of the metal (e.g., between approximately 1,065 °C and 1,080 °C for copper). Heating is performed in a reactive gaseous atmosphere, such as an oxidizing atmosphere, for a sufficient time to create a metal/metal oxide eutectic melt, in the copper/oxygen case (see Fig. 1.1), which upon cooling bonds the metal to the substrate. Gas flow rates used are approximately two cubic feet per hour of an argon-oxygen mixture with an oxygen content of approximately 0.04 molar per cent² or between 0.01 and 0.5% a.w.² The big problem was the oxidation and precipitation of copper oxide in the bonded member. To eliminate this problem, it was proposed to heat the copper and ceramic in a vacuum at a pressure no greater than one millibar and a partial oxygen pressure between 0.001 and 0.1 mbars, with the oxygen pressure under 0.005 mbars at the time of cooling.³ This, however, requires expensive equipment, control over the oxygen partial pressure, and, moreover, it could limit mass production.

Nobuyuki et al.⁴ proposed a method that employed the heating of SiN, SiC (4% YrO, 4% Al₂O₃) and AlN (2% YrO, 2% Al₂O₃) in an air atmosphere furnace to produce an oxide layer. On top of this oxide layer an electrolytic tough pitch copper (300-500 ppm oxygen) can be directly bonded by heating in a furnace at 1,075 °C under a nitrogen gas atmosphere.

Information regarding Akihiro et al. work⁵ was received long after the first successfully experiments of direct bonding of copper to alumina ceramic under inert atmosphere, were performed. Their patent idea was that the oxygen contained in the copper member (in a range of 150 to 600 ppm) alone can promote direct bonding of copper to alumina ceramic layer.

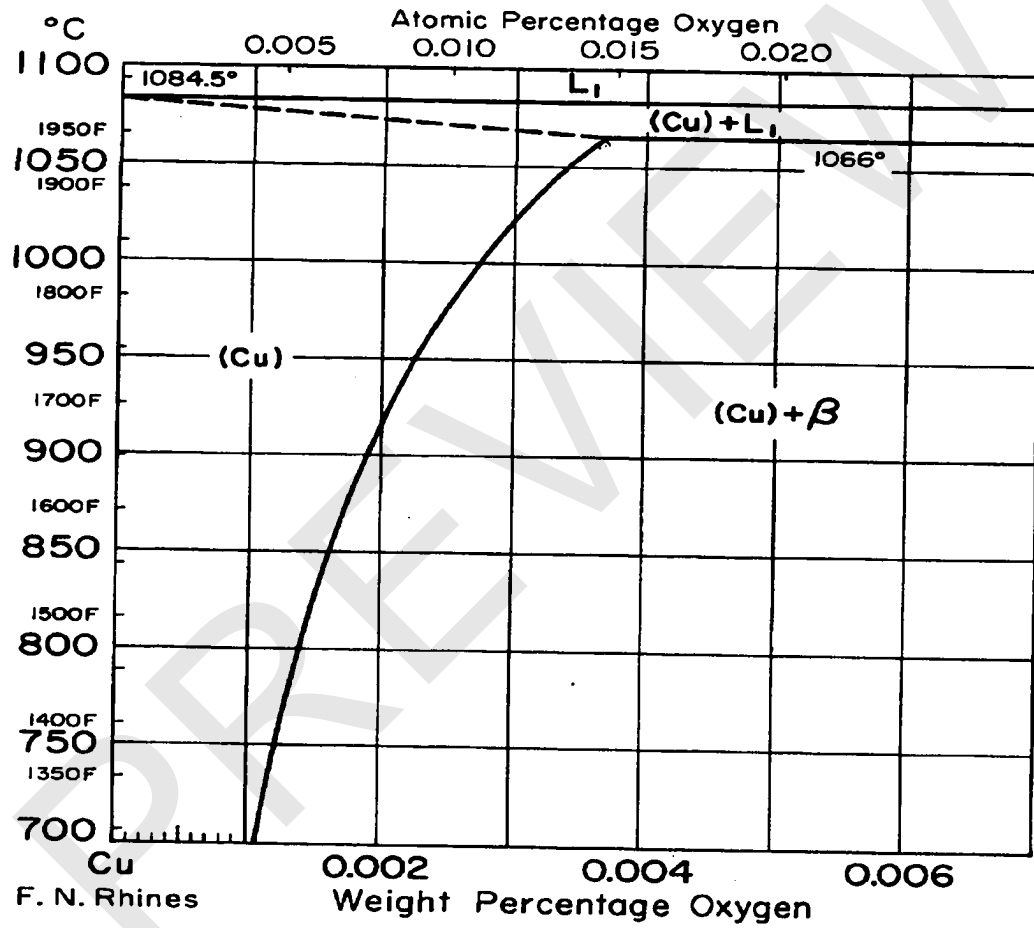


Figure 1.1: Phase diagram of the Cu - O system.